An Acad Bras Cienc (2023) 95(Suppl. 1): e20210859 DOI 10.1590/0001-3765202320210859
Anais da Academia Brasileira de Ciências | *Annals of the Brazilian Academy of Sciences*
Printed ISSN 0001-3765 I Online ISSN 1678-2690
www.scielo.br/aabc | www.fb.com/aabcjournal

ENGINEERING SCIENCES

Comparative study between 1-way and 2-way coupled fluid-structure interaction in numerical simulation of aortic arch aneurysms

MÁRIO LUIS F. DA SILVA, SAULO DE FREITAS GONÇALVES,
JONATHAS HANIEL, THABATA C. LUCAS & RUDOLF HUEBNER

Abstract: Hemodynamic forces are related to pathological variations of the cardiovascular system, and numerical simulations for fluid-structure interaction have been systematically used to analyze the behavior of blood flow and the arterial wall in aortic aneurysms. This paper proposes a comparative analysis of 1-way and 2-way coupled fluid-structure interaction for aortic arch aneurysm. The coupling models of fluid-structure interaction were conducted using 3D geometry of the thoracic aorta from computed tomography. Hyperelastic anisotropic properties were estimated for the Holzapfel arterial wall model. The rheological behavior of the blood was modeled by the Carreau-Yasuda model. The results showed that the 1-way approach tends to underestimate von Mises stress, displacement, and strain over the entire cardiac cycle, compared to the 2-way approach. In contrast, the behavior of the variables of flow field, velocity, wall shear stress, and Reynolds number when coupled by the 1-way model was overestimated at the systolic moment and tends to be equal at the diastolic moment. The quantitative differences found, especially during the systole, suggest the use of 2-way coupling in numerical simulations of aortic arch aneurysms due to the hyperelastic nature of the arterial wall, which leads to a strong iteration between the fluid and the arterial wall.

Key words: 1-way coupling, 2-way coupling, aortic arch aneurysm, blood flow, fluid-structure interaction.

INTRODUCTION

The global mortality rate from aneurysms located in the aorta is approximately 2.2 per 100,000 inhabitants (Roth et al. 2018). Thoracic aortic artery aneurysms are potentially fatal and their complications, such as rupture, hypovolemic shock, tissue compression, dissection, thromboembolism, and ischemia, have a high mortality rate (Lipp et al. 2020). Degenerative aneurysm of the ascending aorta artery is considered an emergency surgical procedure and its progressive dilatation can quickly reach the aortic arch (Cosentino et al. 2019). In clinical practice, a maximum critical diameter of 5.5 cm is the standard indicator for estimating the risk of rupture (Wang et al. 2021). However, for aneurysms with a diameter less than 5.5 cm, pathophysiological complications can occur, even before surgery, with an incidence of 5-10% (Lipp et al. 2020, Wang et al. 2021). In this regard, decision-making for intervention in aortic aneurysms should not be based only on the

maximum diameter of the cross-section of the aneurysm (Salman et al. 2019). Patients with dissection in smaller diameters and patients with large aneurysms still intact without dissection are reported (Czerny et al. 2019).

From a biomechanical perspective, rupture or dissection of the aneurysm occurs when the stress in the aortic vessel exceeds its wall strength (Campobasso et al. 2018). Because hemodynamic forces are related to pathological variations of the cardiovascular system (Savabi et al. 2020), multiphysical numerical simulations of fluid-structure interaction (FSI) become a useful tool in the investigation of aortic aneurysms.

The non-coupled computational solid stress (CSS) technique, for example, does not consider the hemodynamic effect of pulsatile flow and complacency of the arterial wall (Chandra et al. 2013). Similarly, the computational fluid dynamics (CFD) technique without coupling does not take into account the movement of the arterial wall. Thus, fluid-structure interaction and coupling techniques can contribute to surgical practice and scientific studies since they better simulate the mechanical and physiological behavior of the arterial wall due to the forces generated by flow. One-way coupled fluid-structure interaction is adopted because it requires less computational effort, it is simpler to implement than 2-way FSI, and it does not require full or partial mesh reconstruction (remesh), resulting in a mesh of constant quality (Geronzi et al. 2021, Hirschhorn et al. 2020). However, unlike 2-way FSI, 1-way FSI does not guarantee energy conservation at the interface (Geronzi et al. 2021). The 2-way FSI technique is more accurate for large deflections, where the fluid domain is strongly influenced by structural deformation (Kuchumov et al. 2021), which is the case of blood vessel simulations. In addition, 2-way is transient, more stable, and able to capture the interaction between domains over a given period (Hirschhorn et al. 2020).

Mendez et al. (2018) investigated the non-coupled CSS-CFD technique compared to 2-way FSI in the modeling of aneurysms in the ascending aorta. The results showed that for certain parameters, the simplified CSS-CFD approach is comparable to 2-way FSI. Although differences were found in the spatial distributions of other parameters, such as wall shear stress (WSS) and intraluminal stress, correlation analysis suggests statistical agreement between the approaches. This was probably because changes in the diameter of the aneurysm located in the ascending aorta are not elevated due to the rigidity of the aneurysm wall. Arterial wall stiffness is a determining factor for the agreement of these two approaches in the modeling of aorta aneurysms, which has led to a controversy between the effectiveness of the CSS methodology (Campobasso et al. 2018, Mendez et al. 2018, Lin et al. 2017). This fact will also be reflected in the fluid domain, due to variation in arterial diameter, resulting in an overestimation of wall shear stress in the CFD approach (Lin et al. 2017).

In a comparison between the 1-way and 2-way approaches to abdominal aneurysm, Chandra et al. (2013) concluded that main aortic wall stresses in the 1-way method are underestimated in the entire cardiac cycle, compared to the 2-way method. At the same time, Scotti & Finol (2007) showed that there is an overestimation of only 3% of the maximum wall stress by the 1-way approach. Khe et al. (2016) conducted a comparative study between 1-way and 2-way for brain aneurysms and found that, in general, the values of pressure, stress, strain, and displacement are overestimated in the 1-way FSI approach.

The aortic arch is a region of specific geometric characteristics due to its ramifications, so an aneurysm in this region can change the flow dynamics. Considering the lack of specific studies

available in the literature on aneurysms located in the aortic arch and the divergences between studies regarding numerical approaches to integrate the hemodynamic effects of flow and mechanical behavior of the arterial wall, this study presents a comparative analysis of 1-way and 2-way coupling approaches of fluid-structure interaction for aneurysms in the aortic arch.

MATERIALS AND METHODS

In this study, fluid-structure coupling was performed using two methods: 1-way (or partial coupling) and 2-way (or total coupling). In the 1-way technique, the fluid domain was completely solved and the force on the wall due to flow was then transferred to the solid domain as a boundary condition on the inner wall for its solution. In 2-way coupling, the two domains were solved simultaneously, so that, in the same time step until convergence, the forces in the wall due to hemodynamics calculated in the fluid domain were transferred to the solid domain and the displacements due to mechanical response of the arterial structure resulting from this loading were transferred to the fluid domain.

Geometry and mesh

Geometry for simulation was acquired from computed tomography of the thoracic region of a 74-year-old patient with a healthy thoracic aorta. The procedure was approved by the Research Ethics Committee/Universidade Federal de Minas Gerais (COEP-UFMG) – opinion number 4523374. Multislice images contained in the DICOM (Digital Imaging and Communications in Medicine) files were reconstructed three-dimensionally in InVesalius 3.1 software based on 2D images of the sagittal, coronal, and axial planes. The regions of the ascending aorta, aortic arch, and descending thoracic aorta were selected by means of the thresholding technique to elaborate the three-dimensional geometry. Subsequently, in Autodesk Meshmixer software, a fusiform aneurysm was generated in the aortic arch region with 50% dilation. In this same solid, the arterial wall corresponding to the solid domain was created with 2 mm thickness, which corresponds to anatomical values (García-Herrera & Celentano 2013).

Unstructured hybrid tetrahedral and hexahedral meshes were generated for both domains. A similar characteristic length was maintained in both to ensure coupling between the meshes was 100% in the interface between the domains. The meshes were more refined in the region of the aortic arch. The fluid domain mesh has ten refinement layers close to the wall, where it was guaranteed that the first layer had $y^+ \geq 1$. For the grid independence test of the fluid domain, the ASME V&V 20 (ASME 2009) standard was followed, with refinement factor 1.3. The solid domain mesh was refined by the same factor as the fluid domain. Velocity and von Mises stress were monitored for the fluid and solid domains, respectively, at different points of the arch. As a criterion for selection, it was adopted the grid convergence index (GCI) value of less than 5% in all monitored points.

The selected mesh of the fluid domain had 1,073,561 elements and 352,781 nodes and the mesh of the solid domain had 99,674 elements and 171,964 nodes.

A time independence study was done by dividing the time step by half for each simulation until the same variables analyzed in the mesh independence test reached a difference less than 5%. In both approaches, the time step adopted according to the time independence test was 0.01 s. Five cardiac

cycles were simulated to account for numerical instability, transient effects, and independence of initial conditions. The last cycle (4.0 to 5.0 s) was taken for analysis.

Boundary conditions

For the fluid domain, a no-slip condition was applied at the wall, pulsatile mass flow at the inlet of the aorta (i.e. ascending aorta), and pressure pulse at the outlets (i.e. brachiocephalic trunk, left common carotid artery, left subclavian artery, and descending thoracic aorta). The boundary conditions, adapted from Alastruey et al. (2016), are shown in Figure 1a. In addition, turbulence intensity was assumed to be 5% at the inlet and outlet. Figure 1b shows the geometry for simulation as well as the planes selected for analysis of results. For the solid domain, zero displacements were imposed on the faces adjacent to the inlet and outlets sections (Savabi et al. 2020).

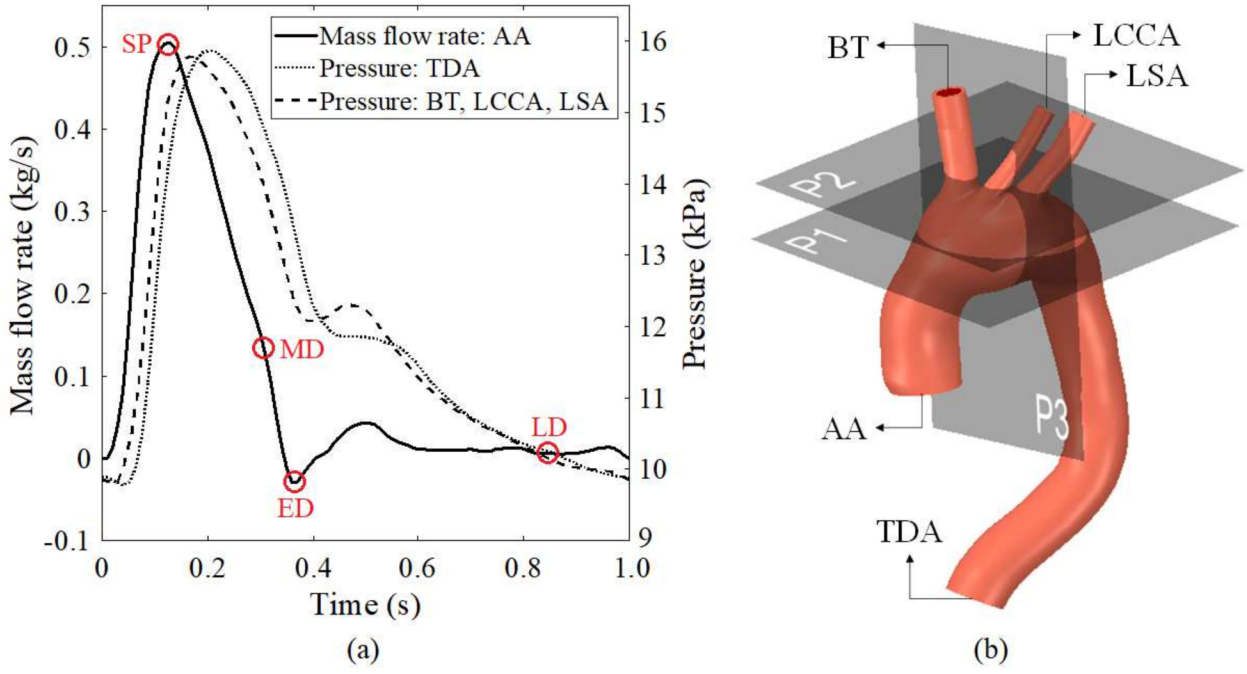

Figure 1. Boundary conditions and planes for post processing. (a) Mass flow and pressure pulses. (b) Cutting planes for results analysis. AA: ascending aorta; TDA: thoracic descending aorta; TB: brachiocephalic trunk; LCCA: left common carotid artery; LSA: left subclavian artery; SP: systolic peak; MD: maximum deceleration; ED: early diastole; LD: late diastole.

For FSI interface, the displacements of fluid and solid must be equal:

$$\mathbf{d_f} = \mathbf{d_s} \tag{1}$$

where $\mathbf{d}$ is the displacement, and s and f represent the solid and fluid domains, respectively. Moreover, stress in both domains must be in balance:

$$\mathbf{n} \cdot \boldsymbol{\tau}_\mathbf{f} = \mathbf{n} \cdot \boldsymbol{\tau}_\mathbf{s} \tag{2}$$

where $\boldsymbol{\tau}_\mathbf{f}$ and $\boldsymbol{\tau}_\mathbf{s}$ are the stresses in the FSI interface, corresponding to the fluid and solid domains, respectively, and $\mathbf{n}$ is the outward normal vector.

For the 1-way approach, the pressure curve on the wall along the cardiac cycle resulting from CFD rigid wall simulation was recorded and subsequently applied as a boundary condition on the inner wall of the artery.

Equations of government

The flow was assumed incompressible, isothermal, and transient. The conservation of mass and conservation of the momentum equations are given by equations 3 and 4, respectively.

$$\nabla \cdot \mathbf{u} = 0 \tag{3}$$

$$\rho_f \left(\frac{\partial \mathbf{u}}{\partial t} + (\nabla \cdot \mathbf{u}) \cdot \mathbf{u} \right) = -\nabla p + \nabla \boldsymbol{\tau} \tag{4}$$

where ρ_f is the density of blood, p is the pressure, t is the instant of time, $\boldsymbol{\tau}$ is the viscous stress tensor, and $\mathbf{u}$ is the flow velocity vector.

The k-ω SST turbulence model was adopted - a hybrid model that has the advantages of the k-ε model for regions away from the wall and the standard k-ω model for regions close to the wall.

The Carreau-Yasuda rheological model (Equation 5) was adopted to represent blood viscosity as a non-Newtonian shear thinning fluid.

$$\mu = \mu_\infty + (\mu_0 - \mu_\infty) \left(1 + (\lambda \dot{\gamma})^a\right)^{\frac{n-1}{a}} \tag{5}$$

where $\dot{\gamma}$ is the shear rate, μ_0 is the zero-shear stress viscosity, μ_∞ is the infinite shear stress viscosity, a is the Yasuda constant, λ is a time constant, and n is the power law index. The adopted values were μ_0 = 0.056 Pa.s, μ_∞ = 0.0035 Pa.s, a = 2, λ = 3.3130 s, and n = 0.03568 (Cho & Kensey 1991). For density, the value of 1060 kg/m^3 was adopted (Yeh et al. 2018).

For the solid domain, the Lagrangian coordinate system was adopted:

$$\nabla \cdot \boldsymbol{\sigma}_\mathbf{s} = \rho_s \dot{\mathbf{u}}_\mathbf{g} \tag{6}$$

where $\boldsymbol{\sigma}_\mathbf{s}$ is the solid stress tensor, ρ_s is the density of the arterial wall, and $\dot{\mathbf{u}}_\mathbf{g}$ is the local acceleration vector.

The arterial wall was modeled as anisotropic hyperelastic, based on the Holzapfel model (Holzapfel et al. 2000), with the following energy density function:

$$W = \frac{C_{10}}{2} \left(\bar{I_1} - 3\right) + \frac{k_1}{2k_2} \sum_{i=4,6} \left(e^{k_2 (\bar{I_1} - 1)^2} - 1 \right) \tag{7}$$

where $\bar{I_4}$ and $\bar{I_6}$ are the pseudo-invariants of the Cauchy-Green tensor. C_{10}, k_1, and k_2 are the constants of the material.

The parameters of the material were calculated according to the work of Huh et al. (2019), which relates these parameters to age of the patient. The values used were: C_{10} = 0.218 MPa, k_1 = 0.16437 MPa, and k_2 = 4.1787.

Numerical solution

The fluid domain was discretized by the finite volume method in Fluent software (ANSYS 2019 R2) and the solid domain was discretized by the finite element method in ANSYS Mechanical software (ANSYS 2019 R2). In the 2-way FSI approach, domain coupling was performed by System Coupling software (ANSYS 2019 R2). Spatial pressure discretization was performed by the second-order central differencing scheme. The spatial discretization of the gradients was performed by the least squares cell-based method. The spatial discretization of momentum, turbulence kinetic energy (k), and specific turbulence dissipation (ω) was performed by the second order upwind method. The spatial discretization of continuity was based on Rhie & Chow (1983). Velocity and pressure coupling was performed using the Coupled algorithm. Finally, temporal discretization was performed by the second-order backward difference method.

For the fluid domain, the convergence criterion of 10^{-4} was adopted for the components of velocity, continuity, k, and ω. For the solid domain, the Newton-Raphson method was used with a residual value of 0.1% of the applied load as a convergence criterion. For the 2-way approach, the convergence criterion was root mean square (RMS) of 10^{-3} for a normalized value of all data transferred between two successive iterations.

Results verification

To verify the results, a numerical simulation was performed in a domain representing the healthy aorta, without aneurysm, by the 2-way approach, following the same methodology described in the approach comparisons. The results for flow along the cardiac cycle in the left common carotid artery were compared with two *in vivo* experimental studies by magnetic resonance imaging (MRI) measurements in healthy aortic patients available in the literature (Boccadifuoco et al. 2018, Olufsen et al. 2000).

RESULTS

The results were post processed in the planes shown in Figure 1b, P1, P2, and P3. The P2 plane cuts the branches of the aortic arch, while the P1 and P3 planes cut the section of the aorta corresponding to the arch in different directions. In addition, the instants of time highlighted in Figure 1a were used in specific analyses: systolic peak (SP), maximum deceleration (MD), early diastole (ED), and late diastole (LD).

Solid domain

The graphs in Figure 2 show the variation of von Mises stress, displacement, and strain along the cardiac cycle in the planes shown in Figure 1b for the 1-way and 2-way approaches. The maximum and average values of these variables in the planes are shown. Table I shows the numerical difference between the approaches for the variables in Figure 2, with the mean absolute percentage deviation (MAPD) of the 1-way approach in relation to the 2-way approach. Moreover, Table I shows the maximum absolute difference (MAD) and the instant of time (t_{MAD}) of such difference.

Table I. Difference of solid variables of 1-way in relation to the 2-way approach in planes P1, P2, and P3. MAPD: mean absolute percentage deviation; MAD: maximum absolute difference; tMAD: instant of time of maximum absolute difference.

Surface	von Mises stress			Displacement			Strain		
	MAPD (%)	MAD (kPa)	t_{MAD} (s)	MAPD (%)	MAD (mm)	t_{MAD} (s)	MAPD (%)	MAD	t_{MAD} (s)
Plane 1	12.1	28400	0.18	11.2	0.569	0.23	11.8	0.021	0.18
Plane 2	4.94	4.94	0.12	10.7	0.613	0.08	6.01	0.005	0.12
Plane 3	8.76	23400	0.21	6.35	0.427	0.21	8.72	0.017	0.18

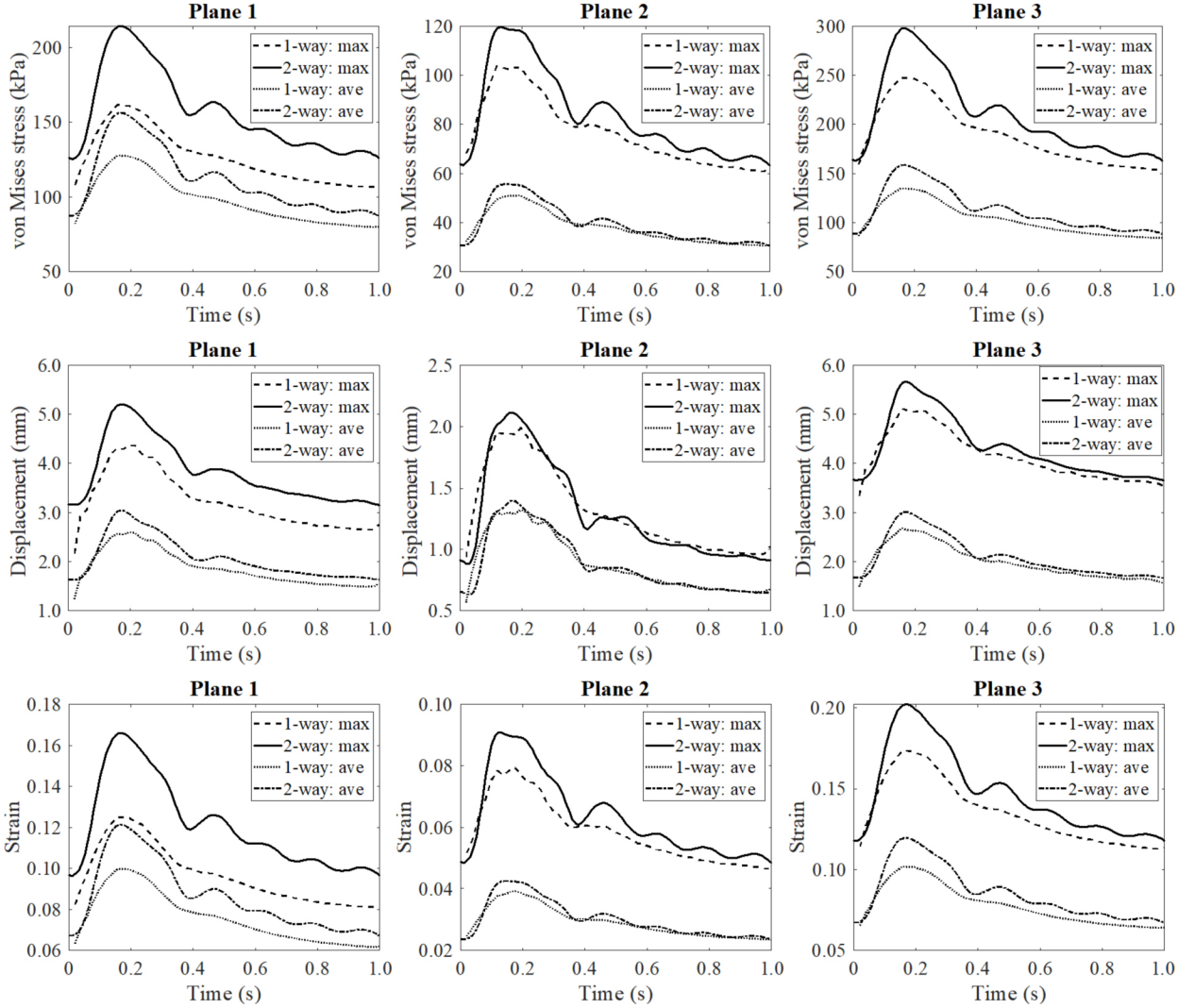

Figure 2. Variation of von Mises stress, displacement, and strain through the cardiac cycle in planes 1, 2, and 3 for the 1-way and 2-way approaches. max: maximum; ave: average.

The P1 plane had the greatest von Mises stress and strain differences, although it did not have the greatest efforts (P3). In contrast, P2 showed the smallest differences, possibly because it was the least requested mechanically. Regarding displacement, in P2, the value in the 1-way approach exceeded that of the 2-way approach in some points. In absolute terms, although the P2 plane had the smallest displacement, it showed the greatest difference between the approaches, as shown in Table I.

According to Figure 2 and Table I, the greatest mechanical stresses and the greatest differences between approaches occurred at or near the systolic peak. In contrast, the smallest differences occur in LD, where the efforts are smaller. For better visualization and comparison of the distribution of von Mises stress and displacement in the aortic arch, Figures 3a-b respectively show the behavior of these variables in PS and LD.

For both approaches, maximum von Mises stress and displacement points occurred at the systolic peak on the inner surface of the artery, as shown in Figure 3c-d, respectively.

Fluid domain

The graphs in Figure 4 show the variation of the mean fluid velocity through the cardiac cycle in the planes P1 and P3 for the 1-way and 2-way approaches. Figure 4 also shows the mean variation of pressure and WSS for both methodologies. Finally, Figure 4 shows the mean variation of viscosity in plane P1 and Reynolds number (Re) in planes P1 and inlet. Re was calculated based on the hydraulic diameter, the mean fluid velocity, and the average viscosity of the analyzed planes. Due to the boundary conditions imposed on the inlet, the Re on this surface is the same in both methodologies.

Table II shows the numerical difference between the approaches for the variables in Figure 4.

The major difference in Re between the approaches was detected in systolic phase. The difference of Re in the plane P1 was mainly due to the velocity difference in this plane, being greater in the 1-way approach as well as due to the difference in viscosity, which is smaller in the 1-way. The maximum Re of the 1-way approach in the plane P1 is comparable to that of the inlet surface, because although the mean velocity in the P1 was lower, the hydraulic diameter is greater.

The mean Womersley number (Wo) was also calculated, based on the mean hydraulic diameter and mean viscosity along the cycle at the inlet and plane P1. At the inlet, Wo = 12.7, at P1 in the 1-way, Wo = 27.7, and at P1 in the 2-way Wo = 30.2. The Wo was greater in the 2-way methodology because the mean hydraulic diameter is greater in this methodology due to lumen deformation.

As presented in the graphs in Figure 4, velocity and WSS show differences throughout the cardiac cycle. Figure 5a shows the velocity streamlines at the points of SP, MD, and ED. The streamlines were drawn starting from the ascending thoracic aorta in the SP and MD instants, and from the descending thoracic aorta in the ED instant, which is the instant near the closure of the aortic valve, where the blood tends to return to the ascending aorta from the descending one. Figure 5b shows the behavior of the WSS at the moments of SP and MD.

Figure 6 shows the variation of the lumen area in P1 according to the local pressure variation. Time runs counterclockwise from the curve. Hysteresis occurs at the moment of systolic peak. There is an area increase that is almost linear with pressure. Area reduction does not occur in a single step due to the variation in pressure that occurs with the events of the cardiac cycle, such as closing of the aortic valve and the systolic phase.

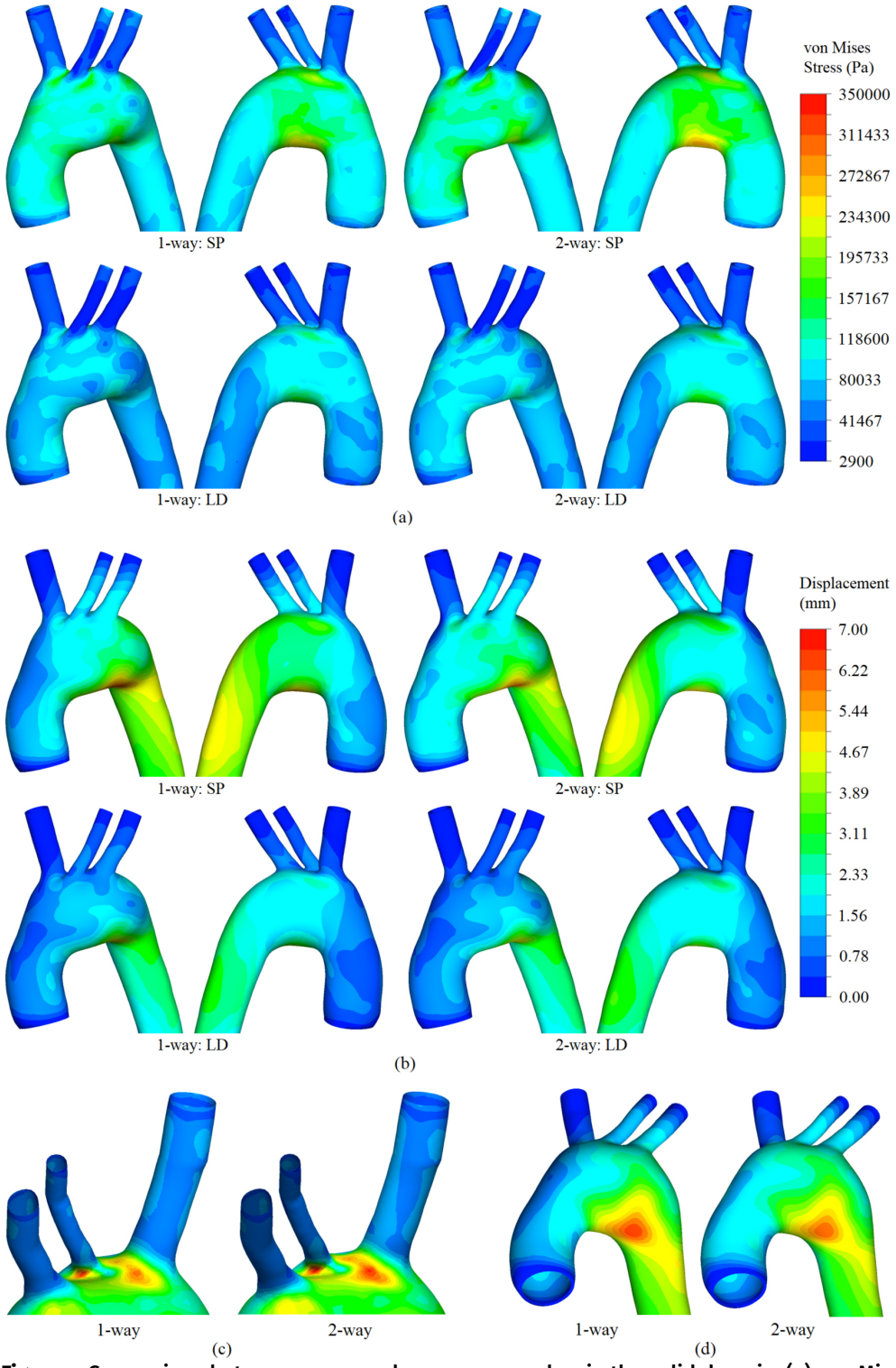

Figure 3. **Comparison between 1-way and 2-way approaches in the solid domain. (a) von Mises stress in SP and LD. (b) Displacement in SP and LD. (c) Highlight of maximum von Mises stress points. (d) Highlight of maximum displacement points.**

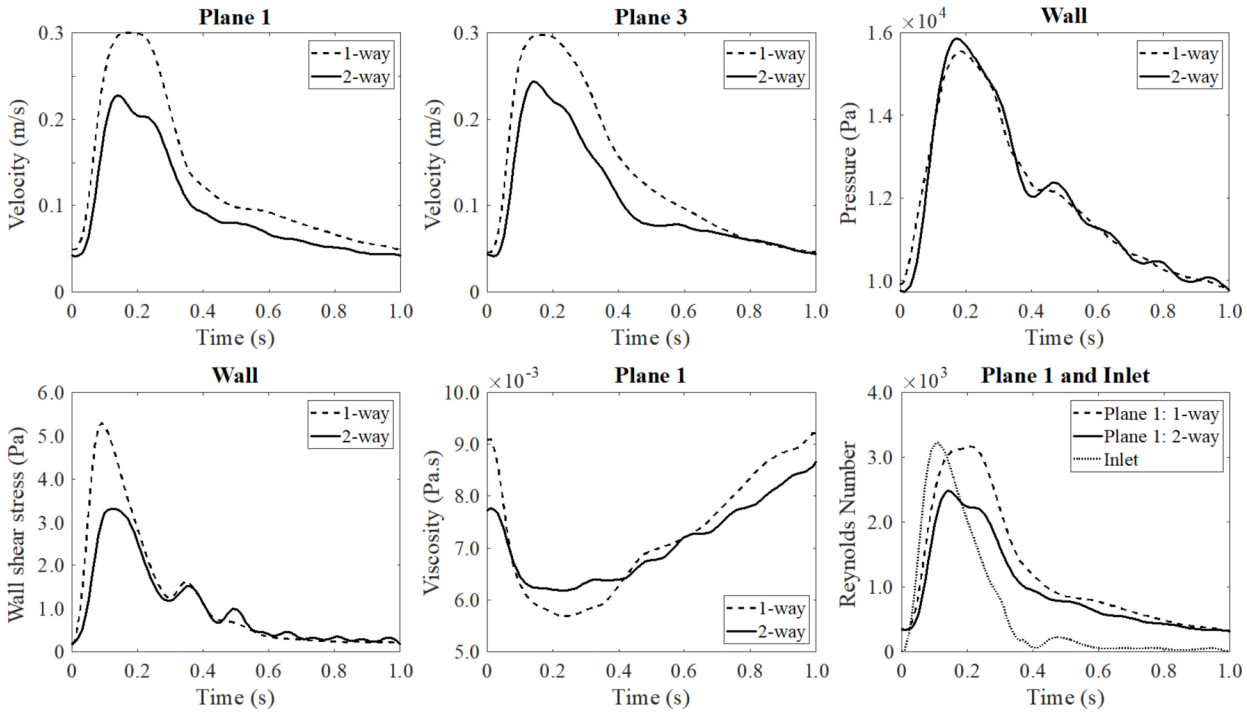

Figure 4. Velocity variation in planes P1 and P3, pressure and WSS variations in the wall, viscosity variation in plane P1, Re variation in planes P1 and inlet through the cardiac cycle for the 1-way and 2-way approaches.

Results verification

Comparative results are shown in Figure 7a in effective values, while in Figure 7b, the values were dimensionless by the maximum volume flow rate of each case.

DISCUSSION

Solid domain

Considering the solid domain, in general, it is notable that the 1-way approach tends to underestimate the von Mises stress, displacement, and strain in relation to the 2-way methodology, as shown in the graphs in Figure 2. Although this difference between the approaches occurs both in average terms and in relation to the maximum values in the analyzed planes, it is intensified in terms of the maximum values. This difference between approaches regarding the behavior of stresses and deformations is in accordance with the numerical study of Chandra et al. (2013) for aneurysms in the abdominal aorta. In the modeling of carotid atherosclerotic plaques, which is another biological application with a hyperelastic wall, it was also shown that the maximum von Mises stress was significantly lower and the velocity significantly higher in the 1-way methodology compared to the 2-way for different plaque models (Tao et al. 2015).

One of the advantages of numerical simulation is the possibility of analyzing wall stresses, as it is one of the main predictors of adverse events such as rupture and dissection of the arterial wall and cannot be measured directly *in vivo* (Xuan et al. 2018, Mendez et al. 2018). As in the case of aneurysms

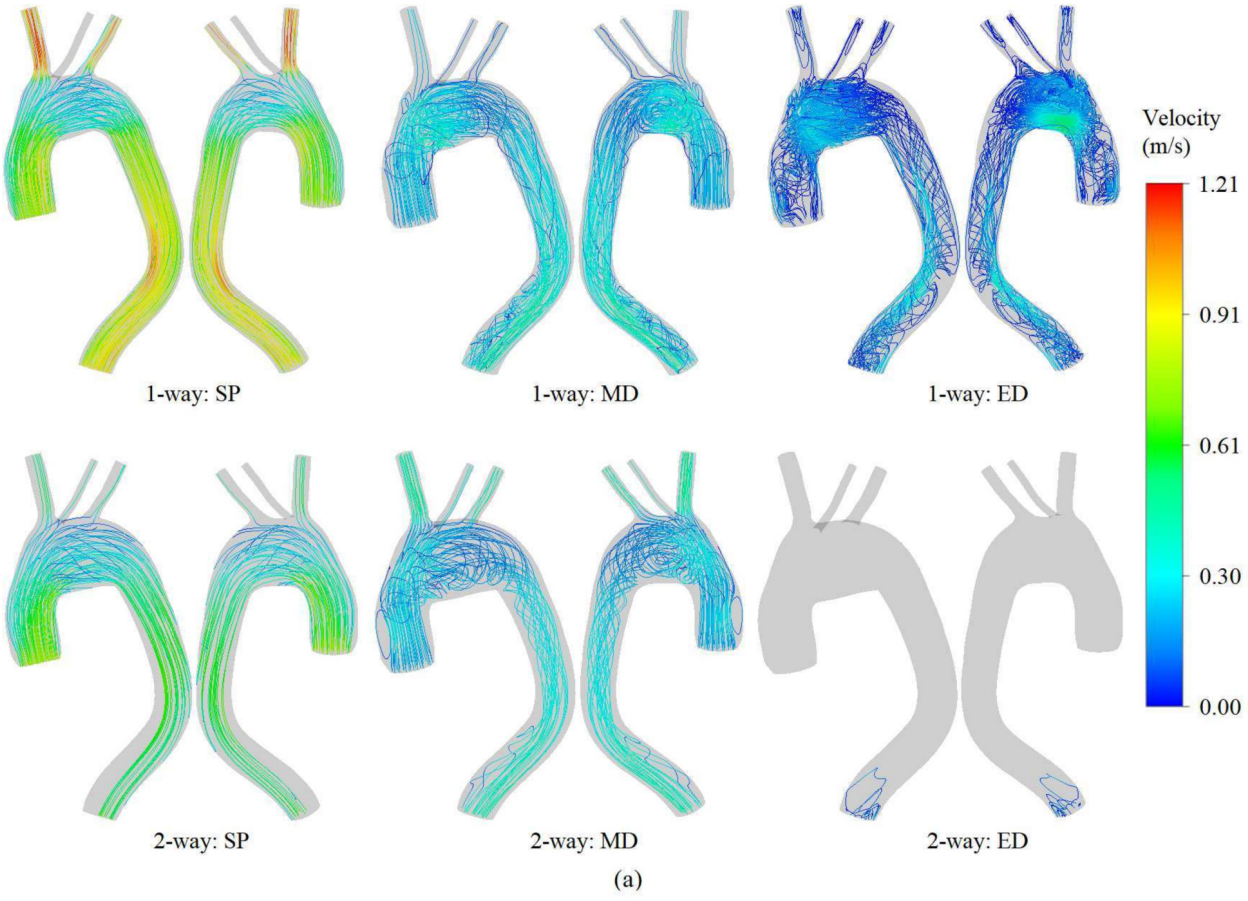

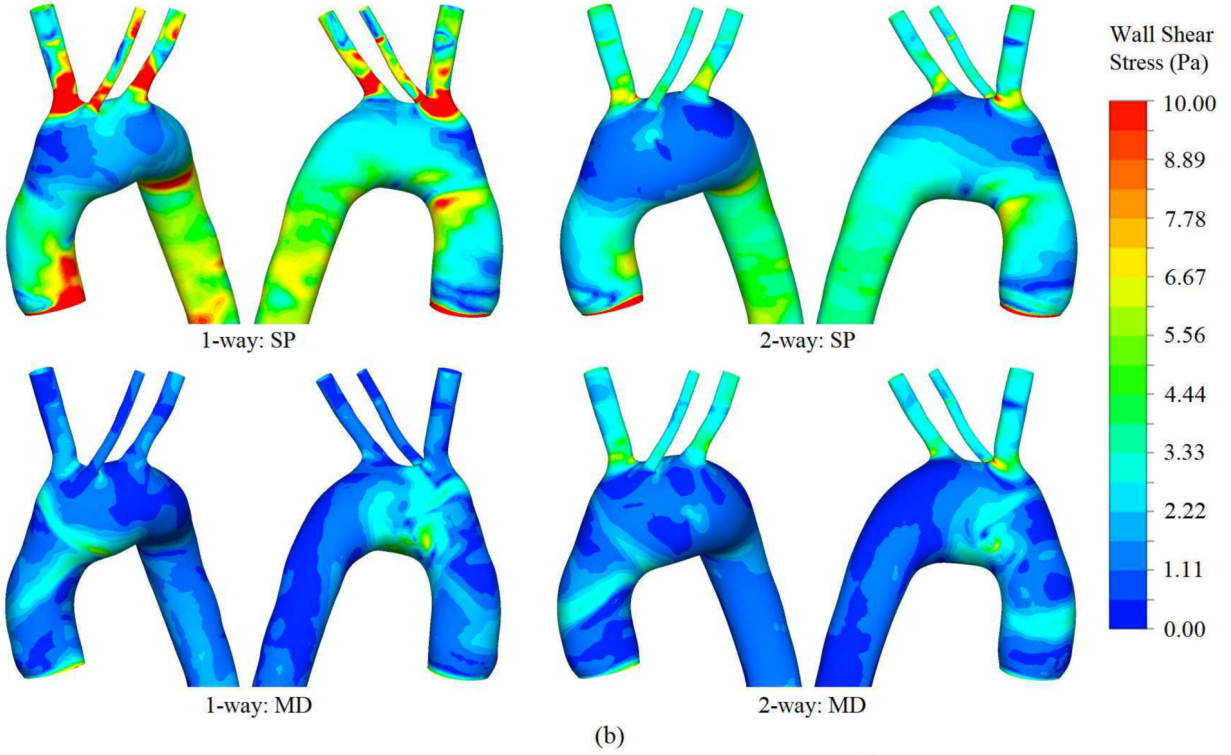

Figure 5. Comparison between 1-way and 2-way approaches in the fluid domain. (a) Velocity streamlines in SP, MD, and ED. (b) Wall shear stress in SP and MD.

Table II. Difference of fluid variables of 1-way in relation to the 2-way approach in planes P1 and P3 and in the wall. MAPD: mean absolute percentage deviation; MAD: maximum absolute difference; tMAD: instant of time of maximum absolute difference.

		Plane 1	Plane 3	Wall
Velocity	**MAPD (%)**	33.200	27.700	-
	MAD (m/s)	0.097	0.087	-
	t_{MAD} (s)	0.200	0.070	-
Pressure	**MAPD (%)**	-	-	1.690
	MAD (Pa)	-	-	1260
	t_{MAD} (s)	-	-	0.050
WSS	**MAPD (%)**	-	-	31.800
	MAD (Pa)	-	-	2.900
	t_{MAD} (s)	-	-	0.070
Viscosity	**MAPD (%)**	5.300	-	-
	MAD (Pa.s)	0.00135	-	-
	t_{MAD} (s)	0	-	-
Re	**MAPD (%)**	22.100	-	-
	MAD	968	-	-
	t_{MAD} (s)	0.210	-	-

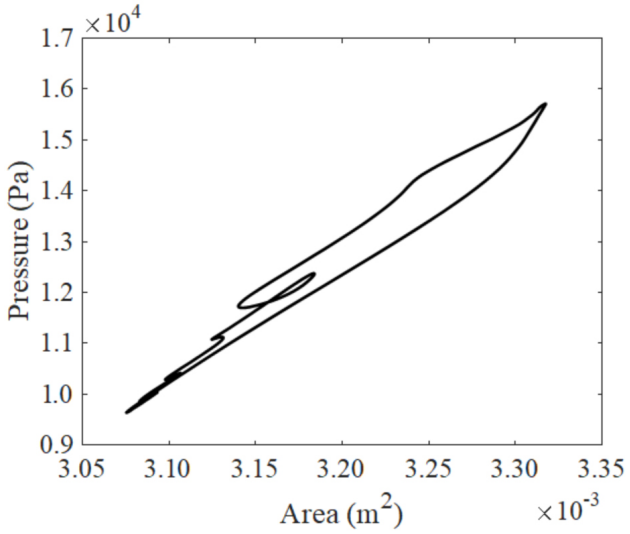

Figure 6. Variation of the area according to the local pressure in plane P1.

in the ascending thoracic aorta (da Silva et al. 2022, Wang et al. 2021, Cosentino et al. 2019, Xuan et al. 2018, Campobasso et al. 2018) and abdominal (Miller et al. 2020, van Disseldorp et al. 2020)

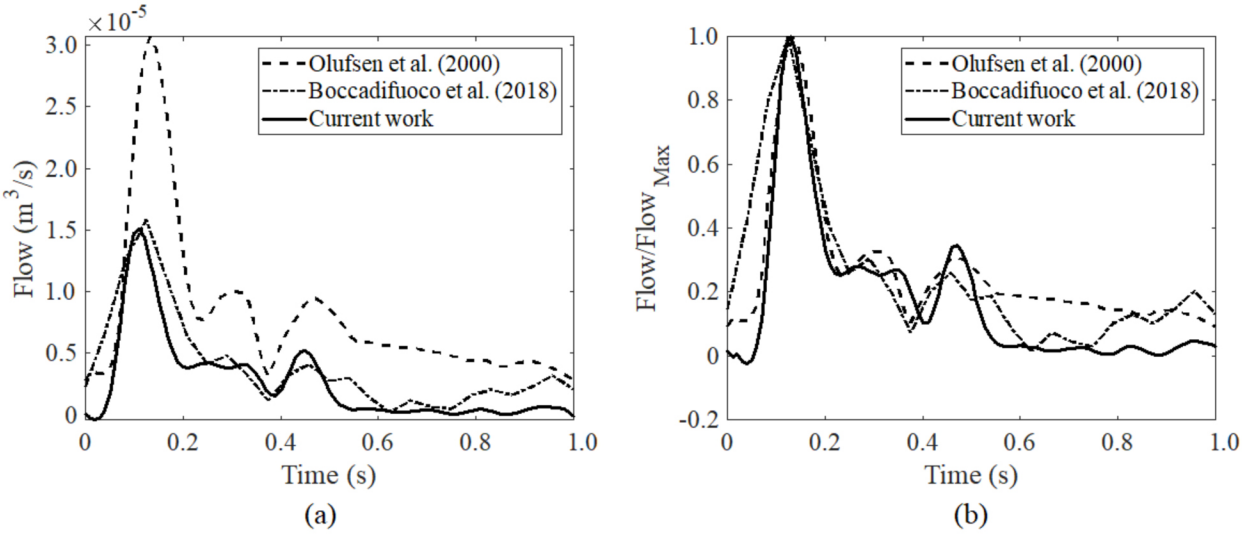

Figure 7. Verification of numerical simulations with experimental data available in the literature for healthy aorta. Volume flow in the left common carotid artery. (a) Effective values. (b) Dimensionless.

and even cerebral aneurysms (Khe et al. 2016), in the aneurysm region, there was an increase in wall stress, herein quantified by von Mises stress. However, peak stress did not occur in the larger diameter aneurysm section, but in the aneurysm neck at the beginning of the branches (Figure 3). Peak stress may be related to the local anatomical curvature of the region (de Galarreta et al. 2017), which explains the occurrence of the peak stress in the aneurysm necks, or in regions of inflection, as observed in numerical analyses of different types and locations of aneurysms (da Silva et al. 2022, de Lucio et al. 2021, Plonek et al. 2017).

Although Table I shows that the maximum MAPD of von Mises stress was 12.1% in the analyzed planes, in terms of maximum values specifically, the difference between the two approaches can be significant, particularly in the systolic peak; therefore, the 1-way approach can lead to an underestimated prediction in the analysis of rupture of the aneurysm. Quantitatively, the stresses found here are in accordance with those of other studies of aneurysms in the thoracic region (Wang et al. 2021, Yeh et al. 2018).

Although the maximum displacements found were high and occurred in the aneurysmal region, the displacements in the other sites of the aorta were within the physiological range for healthy aorta, measured by MRI (Nasr et al. 2017).

Fluid domain

Although the greatest differences in the variables in the solid domain reached 12.1%, in the fluid domain the differences in velocity at P1 and WSS on the wall reached 33.2% and 31.8%, respectively. In P1 and P3, the velocity in the systolic phase of the 1-way approach tended to overestimate the values of the 2-way approach, while in the systolic phase, they tended to approach it. Velocity results are in line with the studies that demonstrated that CFD methodology overestimated the maximum velocity in ascending aortic aneurysm (Nannini et al. 2021) and in thoracic aorta of Marfan syndrome patients (Pons et al. 2020) compared to the 2-way FSI methodology. Furthermore, according to Nannini et al.

(2021) and Pons et al. (2020) the 2-way FSI approach outperform CFD simulations significantly when compared with *in vivo* measurements by 4D phase contrast magnetic resonance imaging (4D PC-MRI). The events of the cardiac cycle vary according to the approach adopted, as can be observed in Figure 5 at the instant of ED. In this instant of time in the 1-way methodology, the blood is already in a more advanced stage of blood return, while in the 2-way methodology, this return event is at its beginning.

The Re computed at inlet were within the physiological range calculated based on data obtained by MRI by Ha et al. (2018) in healthy aorta, being more consistent with Re measured in elderly patients, which is the case of the geometry used in this study. The transition to turbulence that occurs in aneurysms is more related to the deceleration of the flow that makes it unstable than to the Re (Philip et al. 2021, Saqr et al. 2020). The region of the aneurysmal sac becomes conducive to the formation of vortices and greater recirculation, as shown at the instant of MD in the 2-way approach. According to Philip et al. (2021) the vortex formation mechanism is influenced by the wall movement. In rigid arterial walls the vortex pattern is formed only by temporal deceleration while elastic arterial walls generate vortex separation due to wall movement as well as recirculation zones in the center of the aneurysm (Philip et al. 2021, Sharzehee et al. 2018). Vortex formation and flow recirculation mainly in late systole and pre diastole were also verified in thoracic aneurysms by other authors (da Silva et al. 2022, Ong et al. 2018, Nardi & Avrahami 2017). Local blood recirculation may be one of the causes of aneurysm rupture (Numata et al. 2016). The formation of vortices can increase the stress in the blood elements and activate thrombus-causing particles such as platelets, which, together with the recirculation of these elements that occurs in the aneurysmal sac, can lead to the formation of intraluminal thrombus (ILT) (Ong et al. 2018). Ong et al. (2018) conducted a CFD study to investigate the formation of ILT in thoracic aneurysms and found that aortic curvature and aneurysm size are the main contributing factors of persistent vortices during systole that lead to the formation of ILT (Ong et al. 2018). The reduction in the size of aneurysms delays the formation of the vortex and causes it to dissipate earlier, reducing the time of exposure of blood elements to high shear stresses within the vortex (Ong et al. 2018). Figure 5 shows the effect of 2-way modeling, especially in the instants of greater efforts in the arterial wall (SP and MD), where the lumen is more dilated in the 2-way approach, unlike the 1-way methodology where the lumen is constant. Consideration of the lumen without dilation, as occurs in the 1-way methodology, can lead to an underestimation in the formation of the ILT.

WSS was overestimated by the 1-way approach compared to the 2-way in the SP and tended to equalize in the diastolic phase, which was also verified by Chandra et al. (2013) for abdominal aneurysms. This higher value of WSS mainly in the necks and branches can be explained by the non-dissipation of energy into the arterial wall in 1-way methodology, which increases the turbulent kinetic energy in the region and overestimates the WSS (Lin et al. 2017). Boyd et al. (2016) showed by numerical simulation of ruptured abdominal aortic aneurysms that rupture tends to occur in sites of high blood recirculation where thrombus deposition predominates and not in sites of high pressure and WSS. Moreover, according to Boyd et al. (2016) the rupture occurs in sites of low WSS, which is in line with the studies of Zambrano et al. (2016) and Lozowy et al. (2017) who suggested that low WSS promotes ILT accumulation. The highest WSS values found for both approaches were located in the aneurysm necks and not in the aneurysm sac region, where WSS was low, which agree with the work of Simão et al. (2017) and Nardi & Avrahami (2017). Another high WSS point occurred in the branches

due to the area reduction that, consequently, leads to a velocity variation in this region, which was also verified by Numata et al. (2016), Simão et al. (2017) and Etli et al. (2021).

Although the mean fluid pressure variation in the wall throughout the cardiac cycle was similar in both approaches (Figure 4), it may be necessary to implement the 2-way approach in the case of this type of aortic flow analysis, where the arterial wall has hyperelastic behavior. Even with similar pressure profiles, the different coupling methodologies led to different mechanical responses. The results found here corroborate the work of Ong et al. (2018) and Boyd et al. (2016), as, in the 2-way approach with the dilated aneurysmal region, recirculation and von Mises stresses at the end of systole and beginning of diastole were higher, but WSS was lower mainly in the SP, in comparison with the 1-way approach. This suggests that computational numerical simulation as a means to analyze aneurysms and support decision making for possible intervention by the 1-way approach may underestimate the risk of rupture of thoracic aneurysms.

Given the limitations of the 1-way methodology exposed here, it is worth mentioning that the simulations in this methodology were easier and faster. In this study, simulations in the 1-way approach took approximately 18% of the time compared to the 2-way approach.

Model verification

Figure 7, in terms of model verification with experimental studies of the literature for healthy aorta, primarily shows the variability of flow behavior for this type of application. However, when dimensionless, the volumetric flow tends to follow a certain pattern, which the study developed here was able to reproduce. Even in terms of dimensional values, numerical simulation approaches the results of Boccadifuoco et al. (2018).

Although the results found were coincident with others available in the literature, the limitation of this work lies in the need for experimental validation to compare the accuracy of numerical simulations. Another limitation is the need for a specific experimental study for the analyzed thoracic region to define the parameters of the material since the data available and used here are based on the abdominal section of the aorta. Finally, the aorta was modeled with uniform wall thickness and no boundary condition were considered to model the contact of the arterial wall with other tissues and organs.

CONCLUSION

The present study provided a comparison between the 1-way and 2-way coupled fluid-structure interaction of the blood flow field and the mechanical response of an aneurysm located in the aortic arch. Furthermore, the behavior of the flow field and points of maximum stress and displacement of the arterial wall were investigated, which can support growth analysis, the potential for rupture, and decision-making in the medical practice regarding intervention in aneurysms. The correct modeling of FSI also contributes to the knowledge of the dynamics of the arterial wall that is important for the planning and execution of cardiovascular interventions in the aortic arch, such as thoracic endovascular aortic repair (TEVAR). Regarding the solid domain, an underestimation of the 1-way approach in relation to the 2-way was verified in the mechanical response variables, which tended

to intensify at the moment of systolic peak although, in general, both approaches showed similar behavior qualitatively. In contrast, in the fluid domain, an overestimation of the 1-way approach in relation to the 2-way was verified in velocity, WSS and Re. The results indicated that the 1-way methodology may underestimate the formation of ILT, as well as the dissection and rupture of the aneurysm. Future studies should evaluate the behavior of the arterial wall under the methodology of separately implemented arterial layers, as well as directly assess the potential formation of thrombus in aortic arch aneurysms.

Acknowledgments

The authors would like to thank Conselho Nacional de Desenvolvimento Científico e Tecnológico - CNPq (312982/2017-8). This study was financed in part by the Coordenação de Aperfeiçoamento de Pessoal de Nível Superior - Brazil (CAPES) - Finance Code 001.

REFERENCES

ALASTRUEY J, XIAO N, FOK H, SCHAEFFTER T & FIGUEROA CA. 2016. On the impact of modelling assumptions in multi-scale, subject-specific models of aortic haemodynamics. J R Soc Interface 13(119): 20160073.

ASME PC. 2009. Standard for Verification and Validation in Computational Fluid Dynamics and Heat Transfer: ASME V&V 20-2009. Norma. The American Society of Mechanical Engineers.

BOCCADIFUOCO A, MARIOTTI A, CAPELLINI K, CELI S & SALVETTI MV. 2018. Validation of numerical simulations of thoracic aorta hemodynamics: comparison with in vivo measurements and stochastic sensitivity analysis. Cardiovasc Eng Technol 9: 688-706.

BOYD AJ, KUHN DC, LOZOWY RJ & KULBISKY GP. 2016. Low wall shear stress predominates at sites of abdominal aortic aneurysm rupture. J Vasc Surg 63(6): 1613-1619.

CAMPOBASSO R, CONDEMI F, VIALLON M, CROISILLE P, CAMPISI S & AVRIL S. 2018. Evaluation of peak wall stress in an ascending thoracic aortic aneurysm using FSI simulations: effects of aortic stiffness and peripheral resistance. Cardiovasc Eng Technol 9: 707-722.

CHANDRA S, RAUT SS, JANA A, BIEDERMAN RW, DOYLE M, MULUK SC & FINOL EA. 2013. Fluid-structure interaction modeling of abdominal aortic aneurysms: the impact of patient-specific inflow conditions and fluid/solid coupling. J Biomech Eng 135(8).

CHO YI & KENSEY KR. 1991. Effects of the non-Newtonian viscosity of blood on flows in a diseased arterial vessel. Part 1: Steady flows. Biorheol 28(3-4): 241-262.

COSENTINO F, AGNESE V, RAFFA GM, GENTILE G, BELLAVIA D, ZINGALES M, PILATO M & PASTA S. 2019. On the role of material properties in ascending thoracic aortic aneurysms. Comput Biol Med 109: 70-78.

CZERNY M ET AL. 2019. Current options and recommendations for the treatment of thoracic aortic pathologies involving the aortic arch: an expert consensus document of the European Association for Cardio-Thoracic surgery (EACTS) and the European Society for Vascular Surgery (ESVS). Eur J Cardiothorac Surg 55(1): 133-162.

DA SILVA MLF, DE FREITAS GS & HUEBNER R. 2022. Comparative study of arterial wall models for numerical fluid–structure interaction simulation of aortic arch aneurysms. J Braz Soc Mech Sci Eng 44(5): 172.

DE GALARRETA SR, CAZÓN A, ANTÓN R & FINOL EA. 2017. The relationship between surface curvature and abdominal aortic aneurysm wall stress. J Biomech Eng 139(8): 081006.

DE LUCIO M, GARCÍA MF, GARCÍA JD, RODRÍGUEZ LER & MARCOS FÁ. 2021. On the importance of tunica intima in the aging aorta: a three-layered in silico model for computing wall stresses in abdominal aortic aneurysms. Comput Methods Biomech Biomed Engin 24(5): 467-484.

ETLI M, CANBOLAT G, KARAHAN O & KORU M. 2021. Numerical investigation of patient-specific thoracic aortic aneurysms and comparison with normal subject via computational fluid dynamics (CFD). Med Biol Eng Comput 59: 71-84.

GARCÍA-HERRERA CM & CELENTANO DJ. 2013. Modelling and numerical simulation of the human aortic arch under in vivo conditions. Biomech Model Mechanobiol 12: 1143-1154.

GERONZI L, GASPAROTTI E, CAPELLINI K, CELLA U, GROTH C, PORZIANI S, CHIAPPA A, CELI S & BIANCOLINI ME. 2021. High fidelity fluid-structure interaction by radial basis

functions mesh adaption of moving walls: a workflow applied to an aortic valve. J Comput Sci 51: 101327.

HA H, ZIEGLER M, WELANDER M, BJARNEGÅRD N, CARLHÄLL CJ, LINDENBERGER M, LÄNNE T, EBBERS T & DYVERFELDT P. 2018. Age-related vascular changes affect turbulence in aortic blood flow. Front Physiol 9: 36.

HIRSCHHORN M, TCHANTCHALEISHVILI V, STEVENS R, ROSSANO J & THROCKMORTON A. 2020. Fluid–structure interaction modeling in cardiovascular medicine–A systematic review 2017–2019. Med Eng Phys 78: 1-13.

HOLZAPFEL GA, GASSER TC & OGDEN RW. 2000. A new constitutive framework for arterial wall mechanics and a comparative study of material models. J Elast Phys Sci Solid 61: 1-48.

HUH U, LEE CW, YOU JH, SONG CH, LEE CS & RYU DM. 2019. Determination of the material parameters in the Holzapfel-Gasser-Ogden constitutive model for simulation of age-dependent material nonlinear behavior for aortic wall tissue under uniaxial tension. Appl Sci 9(14): 2851.

KHE A, CHEREVKO A, CHUPAKHIN A, BOBKOVA M, KRIVOSHAPKIN A & ORLOV KY. 2016. Haemodynamics of giant cerebral aneurysm: A comparison between the rigid-wall, one-way and two-way FSI models. J Phys: Conf Series 722(1): 012042.

KUCHUMOV AG, VEDENEEV V, SAMARTSEV V, KHAIRULIN A & IVANOV O. 2021. Patient-specific fluid–structure interaction model of bile flow: comparison between 1-way and 2-way algorithms. Comput Method Biomech Biomedic Eng 24(15): 1693-1717.

LIN S, HAN X, BI Y, JU S & GU L. 2017. Fluid-structure interaction in abdominal aortic aneurysm: Effect of modeling techniques. BioMed Res Int 2017: 7023078.

LIPP SN, NIEDERT EE, CEBULL HL, DIORIO TC, MA JL, ROTHENBERGER SM, STEVENS BOSTER KA & GOERGEN CJ. 2020. Computational hemodynamic modeling of arterial aneurysms: a mini-review. Front Physiol 11: 454.

LOZOWY RJ, KUHN DC, DUCAS AA & BOYD AJ. 2017. The relationship between pulsatile flow impingement and intraluminal thrombus deposition in abdominal aortic aneurysms. Cardiovasc Eng Technol 8: 57-69.

MENDEZ V, DI GIUSEPPE M & PASTA S. 2018. Comparison of hemodynamic and structural indices of ascending thoracic aortic aneurysm as predicted by 2-way FSI, CFD rigid wall simulation and patient-specific displacement-based FEA. Comput Biol Med 100: 221-229.

MILLER K ET AL. 2020. Is there a relationship between stress in walls of abdominal aortic aneurysm and symptoms? J Surg Res 252: 37-46.

NANNINI G, CAIMI A, PALUMBO MC, SAITTA S, GIRARDI LN, GAUDINO M, ROMAN MJ, WEINSAFT JW & REDAELLI A. 2021. Aortic hemodynamics assessment prior and after valve sparing reconstruction: A patient-specific 4D flow-based FSI model. Comput Biol Med 135: 104581.

NARDI A & AVRAHAMI I. 2017. Approaches for treatment of aortic arch aneurysm, a numerical study. J Biomech 50: 158-165.

NASR B, LE VEN F, SAVEAN J, SALEM DB, NONENT M, GOUNY P, VISVIKIS D & FAYAD H. 2017. Characterization of the physiological displacement of the aortic arch using non-rigid registration and MR imaging. Eur J Vasc Endovasc Surg 53(2): 282-289.

NUMATA S, ITATANI K, KANDA K, DOI K, YAMAZAKI S, MORIMOTO K, MANABE K, IKEMOTO K & YAKU H. 2016. Blood flow analysis of the aortic arch using computational fluid dynamics. Eur J Cardiothorac Surg 49(6): 1578-1585.

OLUFSEN MS, PESKIN CS, KIM WY, PEDERSEN EM, NADIM A & LARSEN J. 2000. Numerical simulation and experimental validation of blood flow in arteries with structured-tree outflow conditions. An Biomed Eng 28: 1281-1299.

ONG CW, YAP CH, KABINEJADIAN F, NGUYEN YN, CUI F, CHUA KJ, HO P & LEO HL. 2018. Association of hemodynamic behavior in the thoracic aortic aneurysm to the intraluminal thrombus prediction: a two-way fluid structure coupling investigation. Int J Appl Mechs 10(04): 1850035.

PHILIP NT, PATNAIK B & BJ S. 2021. Fluid structure interaction study in model abdominal aortic aneurysms: Influence of shape and wall motion. Int J Num Method Biomed Eng 37(3): e3426.

PLONEK T, ZAK M, BURZYNSKA K, RYLSKI B, GOZDZIK A, KUSTRZYCKI W, BEYERSDORF F, JASINSKI M & FILIPIAK J. 2017. The combined impact of mechanical factors on the wall stress of the human ascending aorta–a finite elements study. BMC Cardiovasc Dis 17(1): 1-7.

PONS R, GUALA A, RODRÍGUEZ-PALOMARES JF, CAJAS J, DUX-SANTOY L, TEIXIDÓ-TURA G, MOLINS JJ, VÁZQUEZ M, EVANGELISTA A & MARTORELL J. 2020. Fluid–structure interaction simulations outperform computational fluid dynamics in the description of thoracic aorta haemodynamics and in the differentiation of progressive dilation in Marfan syndrome patients. R Soc Open Sci 7(2): 191752.

RHIE CM & CHOW WL. 1983. Numerical study of the turbulent flow past an airfoil with trailing edge separation. AIAA J 21(11): 1525-1532.

ROTH GA ET AL. 2018. Global, regional, and national age-sex-specific mortality for 282 causes of death in 195 countries and territories, 1980–2017: a systematic analysis for the Global Burden of Disease Study 2017. Lancet 392(10159): 1736-1788.

SALMAN HE, RAMAZANLI B, YAVUZ MM & YALCIN HC. 2019. Biomechanical investigation of disturbed hemodynamics-induced tissue degeneration in abdominal aortic aneurysms using computational and experimental techniques. Front Bioeng Biotechnol 7: 111.

SAQR KM, TUPIN S, RASHAD S, ENDO T, NIIZUMA K, TOMINAGA T & OHTA M. 2020. Physiologic blood flow is turbulent. Sci Rep 10(1): 15492.

SAVABI R, NABAEI M, FARAJOLLAHI S & FATOURAEE N. 2020. Fluid structure interaction modeling of aortic arch and carotid bifurcation as the location of baroreceptors. Int J Mech Sci 165: 105222.

SCOTTI CM & FINOL EA. 2007. Compliant biomechanics of abdominal aortic aneurysms: a fluid–structure interaction study. Comput Struct 85(11-14): 1097-1113.

SHARZEHEE M, KHALAFVAND SS & HAN HC. 2018. Fluid-structure interaction modeling of aneurysmal arteries under steady-state and pulsatile blood flow: a stability analysis. Comput Method Biomech Biomed Eng 21(3): 219-231.

SIMÃO M, FERREIRA JM, TOMÁS AC, FRAGATA J & RAMOS HM. 2017. Aorta ascending aneurysm analysis using CFD models towards possible anomalies. Fluids 2(2): 31.

TAO X, GAO P, JING L, LIN Y & SUI B. 2015. Subject-specific fully-coupled and one-way fluid-structure interaction models for modeling of carotid atherosclerotic plaques in humans. Med Sci Monit: Int Med J Exp Clin Res 21: 3279.

VAN DISSELDORP EM, VAN DRONKELAAR JJ, PLUIM JP, VAN DE VOSSE FN, VAN SAMBEEK MR & LOPATA RG. 2020. Ultrasound based wall stress analysis of abdominal aortic aneurysms using multiperspective imaging. Eur J Vasc Endovasc Surgy 59(1): 81-91.

WANG Z ET AL. 2021. Wall stress analyses in patients wit ≥ 5 cm versus < 5 cm ascending thoracic aortic aneurysm. The Journal of Thoracic and Cardiovascular Surg 162(5): 1452-1459.

XUAN Y, WANG Z, LIU R, HARALDSSON H, HOPE MD, SALONER DA, GUCCIONE JM, GE L & TSENG E. 2018. Wall stress on ascending thoracic aortic aneurysms with bicuspid compared with tricuspid aortic valve. J Thorac Cardiovasc Surg 156(2): 492-500.

YEH HH, RABKIN SW & GRECOV D. 2018. Hemodynamic assessments of the ascending thoracic aortic aneurysm using fluid-structure interaction approach. Med Biol Eng Comput 56: 435-451.

ZAMBRANO BA, GHARAHI H, LIM C, JABERI FA, CHOI J, LEE W & BAEK S. 2016. Association of intraluminal thrombus, hemodynamic forces, and abdominal aortic aneurysm expansion using longitudinal CT images. An Biomed Eng 44: 1502-1514.

How to cite

SILVA MLF, GONÇALVES SF, HANIEL J, LUCAS TC & HUEBNER R. 2023. Comparative study between 1-way and 2-way coupled fluid-structure interaction in numerical simulation of aortic arch aneurysms. An Acad Bras Cienc 95: e20210859. DOI 10.1590/0001-3765202320210859.

Manuscript received on June 7, 2021;
accepted for publication on December 19, 2022

MÁRIO LUIS F. DA SILVA[1]
https://orcid.org/0000-0002-7817-6191

SAULO DE FREITAS GONÇALVES[1]
https://orcid.org/0000-0002-7011-5108

JONATHAS HANIEL[1]
https://orcid.org/0000-0002-7234-5513

THABATA C. LUCAS[2]
https://orcid.org/0000-0001-7850-8494

RUDOLF HUEBNER[3]
https://orcid.org/0000-0003-2613-304X

[1]Programa de Pós-Graduação em Engenharia Mecânica, Universidade Federal de Minas Gerais, Departamento de Engenharia Mecânica, Avenida Presidente Antônio Carlos, 6627, Pampulha, 31270-901 Belo Horizonte, MG, Brazil
[2]Programa de Pós-Graduação em Ciências da Saúde, Universidade Federal dos Vales do Jequitinhonha e Mucuri, Departamento de Enfermagem, MGC 367, km 583, 5000, Alto da Jacuba, 39100-000 Diamantina, MG, Brazil
[3]Universidade Federal de Minas Gerais, Departamento de Engenharia Mecânica, Avenida Presidente Antônio Carlos, 6627, Pampulha, 31270-901 Belo Horizonte, MG, Brazil

Correspondence to: **Mário Luis Ferreira da Silva**

E-mail: marioluisfs@gmail.com

Author contributions

Mário Luis Ferreira da Silva: Research, paper conception, literature review, methodology, data collection, data analysis and interpretation, paper writing, critical revision and

approval final of article. Saulo de Freitas Gonçalves: Paper conception, literature review, data collection, data analysis and interpretation, paper writing, critical revision and approval final of article. Jonathas Haniel: Paper conception, data analysis and interpretation, paper writing, critical revision and approval final of article. Thabata Coaglio Lucas: Research, literature review, data analysis and interpretation, paper writing, critical revision and approval final of article. Rudolf Huebner: Research, paper conception, methodology, data analysis and interpretation, critical revision and approval final of article.